Geosci. Model Dev. Discuss., 7, C3799–C3836, 2016
www.geosci-model-dev-discuss.net/7/C3799/2016/

Geoscientific Model Development Discussions

Interactive comment on "Northern Hemisphere storminess in the Norwegian Earth System Model (NorESM1-M)" *by* E. M. Knudsen and J. E. Walsh

E. M. Knudsen and J. E. Walsh

erlend.knudsen@gfi.uib.no

Received and published: 29 February 2016

We thank the anonymous reviewer for his/her suggestions on the manuscript. With the changes explained below, we feel that the paper is strengthened compared to its first submission.

In the following, we go through each comment by the reviewers and explain our choices of changes in accordance to these. Where changes to the text in the manuscript are made, the relevant paragraph is reproduced from the .pdf manuscript to this .docx response, with changes written in [brackets].

— 1: RCP4.5 and 2037-2063 inclusions —

We agree with the reviewer in that results for RCP4.5 and 2037-2063 should be in-

cluded in the paper. However, we consider these results secondary to those in the original version of the manuscript. Hence, we have added the results in figures in the Appendix.

Please note that since Figs. A-E are given in the Appendix and not the main body of the manuscript, none of these figures shows significant change or p-values indicating significant change relative to the historical time period for future time periods and scenarios. We believe that Figs. A-E are more compelling without the overlay of the additional information, which complicates the visual presentation of the results.

Added section Appendix B: Additional figures (new text in [brackets]):

<Fig_A.pdf>

[Figure A. Sea ice concentration (a), (f) averages for SOND 1979-2005 and (b), (c), (d), (e), (g), (h), (i), (j) changes in average over various time periods and scenarios relative to 1979– 2005 in NorESM (upper row) and CCSM (lower row). The time periods and scenarios are (b), (g) RCP4.5 2037-2063 – 1979-2005, (c), (h) RCP8.5 2037–2063 – 1979-2005, (d), (i) RCP4.5 2074-2100 – 1979-2005 and (e), (j) RCP8.5 2074-2100 – 1979-2005.]

<Fig_B.pdf>

[Figure B. Sea level pressure (a), (f) averages for SOND (a), (f) 1979-2005 and (b), (c), (d), (e), (g), (h), (i), (j) changes in average over various time periods and scenarios relative to 1979– 2005 in NorESM (upper row) and CCSM (lower row). The time periods and scenarios are (b), (g) RCP4.5 2037-2063 – 1979-2005, (c), (h) RCP8.5 2037–2063 – 1979-2005, (d), (i) RCP4.5 2074-2100 – 1979-2005 and (e), (j) RCP8.5 2074-2100 – 1979-2005.]

<Fig_C.pdf>

[Figure C. Track density (a), (f) averages for SOND (a), (f) 1979-2005 and (b), (c), (d), (e), (g), (h), (i), (j) changes in average over various time periods and scenarios relative

to 1979– 2005 in NorESM (upper row) and CCSM (lower row). The time periods and scenarios are (b), (g) RCP4.5 2037-2063 – 1979-2005, (c), (h) RCP8.5 2037–2063 – 1979-2005, (d), (i) RCP4.5 2074-2100 – 1979-2005 and (e), (j) RCP8.5 2074-2100 – 1979-2005.]

<Fig_D.pdf>

[Figure D. Mean intensity (a), (f) averages for SOND (a), (f) 1979-2005 and (b), (c), (d), (e), (g), (h), (i), (j) changes in average over various time periods and scenarios relative to 1979– 2005 in NorESM (upper row) and CCSM (lower row). The time periods and scenarios are (b), (g) RCP4.5 2037-2063 – 1979-2005, (c), (h) RCP8.5 2037–2063 – 1979-2005, (d), (i) RCP4.5 2074-2100 – 1979-2005 and (e), (j) RCP8.5 2074-2100 – 1979-2005. Regions with track density below 0.5 no. density (month)-1 (106 km2)-1 in the historical time period are shaded white.]

<Fig_E.pdf>

[Figure E. Precipitation (a), (f) averages for SOND (a), (f) 1979-2005 and (b), (c), (d), (e), (g), (h), (i), (j) changes in average over various time periods and scenarios relative to 1979– 2005 in NorESM (upper row) and CCSM (lower row). The time periods and scenarios are (b), (g) RCP4.5 2037-2063 – 1979-2005, (c), (h) RCP8.5 2037–2063 – 1979-2005, (d), (i) RCP4.5 2074-2100 – 1979-2005 and (e), (j) RCP8.5 2074-2100 – 1979-2005.]

Change of 1st paragraph and added new 2nd paragraph in 3 Results and discussion (changes in [brackets]):

In the following, parameters representing storminess are presented. While Sect. 3.1 compares the representations of NorESM and CCSM to ERA-I, Sect. 3.2 shows the expected changes of these parameters towards the end of the century, as projected by NorESM and CCSM. Only the 2074–2100 time period following the RCP8.5 scenario is shown here because of the near linear scaling of changes in sea ice, SLP, [track density,

mean intensity] and precipitation with strength of scenario (RCP4.5 and RCP8.5) and time (1979–2005 to 2037–2063 and 2074–2100) in our results [(Table 1 and Figs. A to E)]. Hence, we consider the 2037–2063 time period to be an intermediate state between the historical and 2074–2100 periods, and the RCP4.5 scenario to be mid-way to the RCP8.5 scenario.

[While the scaling appear more distinct for sea ice, SLP and precipitation, Figs. C and D show signs of similar behaviour for storm frequency and intensity. This is partly in contrast to Catto et al. (2011). Using the HiGEM high-resolution model, they found northeastward shift of the North Atlantic storm track for the intermediate scenario only. In our results, the northeastward shift gets stronger with scenario and time in NorESM (Figs. Ca to Ce and Figs. Da to De). In CCSM, the North Atlantic storm track generally weakens with scenario and time (Figs. Cf to Cj and Figs. Df to Dj). Overall, signals strengthen with scenario and time in both models. These results extend those of Zappa et al. (2013b), who found mean response generally larger, but also more diverging, for RCP8.5 than RCP4.5 in 19 CMIP5 models (not including CCSM).]

New references:

Catto, J., Shaffrey, L., and Hodges, K.: Northern Hemisphere extratropical cyclones in a warming climate in the HiGEM high-resolution climate model, J. Climate, 24, 5336–5352, doi:10.1175/2011JCLI4181.1, 2011.

Zappa, G., Shaffrey, L., Hodges, K., Sansom, P., and Stephenson, D.: A multimodel assessment of future projections of North Atlantic and European extratropical cyclones in the CMIP5 climate models*, J. Climate, 26, 5846–5862, doi:10.1175/JCLI-D-12-00573.1, 2013b.

— 2: Precipitation changes due to storm track changes —

Change of 1st-2nd paragraph in 3.1.4 Precipitation (changes in [brackets]):

[In terms of broad-scale pattern, precipitation is positively correlated with storminess,

although one cannot say that precipitation is a real measure of storminess. Hawcroft et al. (2012) and Catto et al. (2012) showed the proportion of precipitation associated with extratropical cyclones and fronts, respectively. Only through this type of linkage can a causal relationship be established. In this study, because precipitation per se is not our main focus, we merely point to consistencies between our results and general characteristics of precipitation vis-à-vis its drivers. For example,] cyclone-dense regions are [generally] characterized by high frontal precipitation, with precipitation reaching [especially] high levels [where] cyclones track into mountainous land [so that precipitation is orographically enhanced].

[Figures 4a, Ea and Ef] shows the average pattern of precipitation for NH midlatitudes and high-latitudes over the historical time period. [While climate models generally distinguish convective and non-convective precipitation, their archives do not distinguish frontal and orographic precipitation – two of the primary types of non-convective precipitation. Nevertheless, one can infer that heavy precipitation events in non-mountainous areas have a general association with frontal activity (Kunkel et al. 2012), while precipitation maxima in mountainous areas have a substantial orographic component. Subject to these assumptions, some inferences can be made about the key features that stand out in Fig. 4.] [Sentence moved.]

Change of 2nd paragraph in 3.2.4 Precipitation (changes in [brackets]):

[The reduced precipitation in the eastern North Atlantic Ocean in September coincides with reduced cyclone frequency in CCSM and intensity in both NorESM and CCSM (Figs. 8a and 8b compared to Figs. 6b, 7a and 7b). The correspondence between precipitation and cyclone intensity is consistent with the findings of Zappa et al. (2013b). However, while the changes in storm tracks and precipitation are coherent, this consistency does not prove a causal relationship. The expected drying of the eastern North Atlantic Ocean stems from the poleward migration of the Hadley Cell's downward limb (Kang and Lu, 2012), which is projected to increase dryness in the African-Eurasian region (including the Mediterranean), southwestern North America and northeastern

Brazil (Lau and Kim, 2015). The eastern North Atlantic] is projected to warm less than the rest of the NH, with relatively lower humidity [reducing the] potential for increased atmospheric moisture (Stocker et al., 2013). [In December, the changes of precipitation in the eastern North Atlantic are mostly positive and are not strongly related to storm track changes (Figs. 8c and 8d).]

New references:

Catto, J., Jakob, C., Berry, G., and Nicholls, N.: Relating global precipitation to atmospheric fronts, Geophys. Res. Lett., 39, L10 805, doi:10.1029/2012GL051736, 2012.

Hawcroft, M., Shaffrey, L., Hodges, K., and Dacre, H.: How much Northern Hemisphere precipitation is associated with extratropical cyclones?, Geophys. Res. Lett., 39, L24 809, doi:10.1029/2012GL053866, 2012.

Kang, S. and Lu, J.: Expansion of the Hadley cell under global warming: Winter versus summer, J. Climate, 25, 8387–8393, doi:10.1175/JCLI-D-12-00323.1, 2012.

Kunkel, K., Easterling, D., Kristovich, D., Gleason, B., Stoecker, L., and Smith, R.: Meteorological causes of the secular variations in observed extreme precipitation events for the conterminous United States, J. Hydrometeorology, 13, 1131–1141, doi:10.1175/JHM-D-11-0108.1, 2012.

Lau, W. and Kim, K.-M.: Robust Hadley Circulation changes and increasing global dryness due to CO2 warming from CMIP5 model projections, P. Natl. Acad. Sci. USA, 112, 3630–3635, doi:10.1073/pnas.1418682112, 2015.

Zappa, G., Shaffrey, L., Hodges, K., Sansom, P., and Stephenson, D.: A multimodel assessment of future projections of North Atlantic and European extratropical cyclones in the CMIP5 climate models*, J. Climate, 26, 5846–5862, doi:10.1175/JCLI-D-12-00573.1, 2013b.

— 3: Error discussion —

We agree with the reviewer that comparisons between data sets are made easier when differences rather than separate means are shown. Hence, Figs. 1-4 (b) and (c) now shows NorESM – ERA-I and CCSM – ERA-I instead of NorESM and CCSM historical time period means, respectively. NorESM and CCSM historical means are shown in Figs. A-E (a) and (f).

<Fig_1.pdf>

Figure 1. [Sea level pressure average] for SOND 1979–2005 in (a) ERA-I [and bias of (b) NorESM and (c) CCSM relative to ERA-I. Alternating black and white dots in (b) and (c) mark regions of significant bias at a 95 % confidence level.]

Change of 1st-2nd paragraph in 3.1.1 Sea level pressure (changes in [brackets]):

Under the assumption that ERA-I represents the actual conditions [(Fig. 1a)], NorESM and CCSM reproduce the main SLP pattern [(Figs. Ba and Bf)], but both also show distinct biases [(Figs. 1b and 1c)]. In midlatitudes (here defined 40–65°N), differences are small, with most of the variations due to the representation of the Siberian High (Table 2), which is slightly strengthened and shifted equatorwards in the two models (Fig. 1). This bias is [stronger] in NorESM[, which] represents the Siberian High with SLP up to 1031 hPa compared to the maximum of 1027 hPa in ERA-I.

Contrary to the [equatorward]-shifted Siberian High, the local minima of the Aleutian and Icelandic lows are shifted polewards in the two models, [as represented by the positive (negative) SLP bias south (north) of the pressure system centres in Fig. 1. This coincides with the marked negative bias in high-latitudes (here defined 65–90°N) in both models, where NorESM and CCSM depict 2 and 6 hPa, respectively, lower SLP than ERA-I (Table 2 and Figs. 1b and 1c).]

<Fig_2.pdf>

Figure 2. [Track density average] for SOND 1979–2005 in (a) ERA-I [and bias of (b) NorESM and (c) CCSM relative to ERA-I. Alternating black and white dots in (b) and

(c) mark regions where $p < 0.05$ based on 2000 samples.]

Change of 1st-5th paragraph in 3.1.2 Track density (changes in [brackets]):

[Figures 2a, Ca and Cf] shows the distribution in cyclone frequency in the three data sets. The two main storm tracks of the North Atlantic and the North Pacific oceans are apparent, and likewise the local maxima over Canada and northern Eurasia.

Compared to ERA-I, both models depict poleward-shifted storm tracks over the North Pacific Ocean, Canadian Arctic and the Nordic Seas [(Figs. 2b and 2c)]. On the contrary, the eastern branch of the North Atlantic storm track is broader and extends farther south in the models. These features offer an explanation for the poleward-shifted and wider low SLP bands in Fig. 1. For the North Atlantic Ocean overall, cyclones in NorESM and CCSM are slightly too zonal compared to ERA-I, consistent with the winter pattern found in CMIP5 models by Zappa et al. (2013a). This leaves fewer cyclones tracking through the Greenland Sea âĂŤ the region where most Arctic cyclones track (Sorteberg and Walsh, 2008). [It is worth mentioning that the zonal North Atlantic storm track bias is stronger in CCSM than in NorESM (Figs. 2b, 2c, Ca and Cf). This coincides with a SIC pattern of higher (lower) SIC in the Labrador Sea (Greenland and Barents seas) in CCSM compared to NorESM (Fig. Af compared to Fig. Aa). This SIE anomaly pattern was also found to be associated with weaker and more zonal North Atlantic storm track in CCSM3 during winter (Magnusdottir et al., 2004).]

In CCSM, the number of cyclones within the domain of 40–90°N is 7 % higher than in ERA- I, mainly due to the discrepancy in high-latitudes (Table 2 [and Fig. 2c]). On the contrary, there are 2 % fewer cyclones in NorESM than found in ERA-I [(Table 2 and Fig. 2b)]. For NorESM, this anomaly stems from its resolution, which is about four times as coarse as in the reanalysis. This leaves fewer cyclones resolved (Hodges et al., 2011).

The signal in CCSM offers an additional explanation to the large-scale background SLP

[biases across the main storm tracks] discussed in Sect. 3.1.1. [As] more cyclones are resolved in CCSM compared to ERA-I (Table 2), a particular grid point in the storm track [undergoes] low SLP for more time steps, understandably dependent on the cyclone strength. [For regions of the main storm tracks, this can lower the SLP temporal mean.] This is indicated by the anomalous low SLPs [over the poleward-shifted North Atlantic and North Pacific storm tracks (Figs. 1c and 2c)]. Why CCSM gives more cyclones than ERA-I in the first place is unknown, but might reside in its distribution of sea surface temperature or sea ice, or of different parameterization, e.g., for convection.

Moreover, most of the discrepancy relative to ERA-I stems from the high-latitudes south of the Arctic Ocean, with 14 % more cyclones in CCSM over the band 55–65°N [(Fig. 2c)]. This could point to a closer similarity of CCSM to the Arctic System Reanalysis (ASR) over ERA-I, as found by Tilinina et al. (2014). They detected 28–40 % more cyclones over high-latitude continental areas in summer and winter in the ASR compared to ERA-I and other global modern era reanalyses, ascribing the anomaly mostly to moderately deep and shallow cyclones [(cyclones with central pressure higher than 980 hPa)].

<Fig_3.pdf>

Figure 3. [Mean intensity average] for SOND 1979–2005 in (a) ERA-I [and bias of (b) NorESM and (c) CCSM relative to ERA-I]. Regions with track density below 0.5 no. density (month)-1 (106 km2)-1 are shaded white. [Alternating black and white dots in (b) and (c) mark regions where $p < 0.05$ based on 2000 samples.]

Change of 1st-3rd paragraph in 3.1.3 Mean intensity (changes in [brackets]):

The average strength of cyclones per unit area is presented in [Figs. 3a, Da and Df. This is measured as mean intensity, indirectly linked to spatial changes in wind fields through the horizontal component of relative vorticity.] Since regions of numerous cyclones are likely also to include more intense cyclones than other regions, the mean intensity pattern generally follows the track density pattern in [Figs. 2a, Ca and Cf.

Additionally,] cyclones are stronger over ocean than land. [Dependent clause deleted.]

Corresponding to the [general poleward shift] of the SLP [minima and track density maxima along the two main storm tracks relative to ERA-I (Figs. 1 and 2), NorESM and CCSM have too low mean intensities over the North Atlantic and North Pacific oceans (Figs. 3b and 3c). Conversely, as for track density, positive biases are found over large swaths of Eurasia and western North America, indicating lower contrasts between regions of high and low cyclonic activity in the models compared to ERA-I (Figs. 2b, 2c, 3b and 3c).]

[Model biases are generally more coherent for mean intensity than track density (Figs. 3b and 3c compared to Figs. 2b and 2c), where stronger (weaker) cyclones correspond to lower (higher) SLP (Table 2). However, this relationship does not hold for sea ice-covered areas (Figs. 3b and 3c compared to Figs. 1b and 1c).]

<Fig_4.pdf>

Figure 4. [Precipitation average] for SOND 1979–2005 in (a) ERA-I [and bias of (b) NorESM and (c) CCSM relative to ERA-I. Alternating black and white dots in (b) and (c) mark regions of significant bias at a 95 % confidence level.]

Change of 2nd-5th paragraph in 3.1.4 Precipitation (changes in [brackets]):

[Figures 4a, Ea and Ef] shows the average pattern of precipitation for NH midlatitudes and high-latitudes over the historical time period. [While climate models generally distinguish convective and non-convective precipitation, their archives do not distinguish frontal and orographic precipitation – two of the primary types of non-convective precipitation. Nevertheless, one can infer that heavy precipitation events in non-mountainous areas have a general association with frontal activity (Kunkel et al. 2012), while precipitation maxima in mountainous areas have a substantial orographic component. Subject to these assumptions, some inferences can be made about the key features that stand out in Fig. 4.]

Firstly, frontal precipitation accounts for a large fraction of the precipitation, as seen from the close similarity between the precipitation [(Figs. 4a, Ea and Ef)] and cyclone track density fields [(Figs. 2a, Ca and Cf)]. Secondly, orographic precipitation is the second most important component to the precipitation. This can be seen from the maxima where the main storm tracks reach land (the west coasts of North America, Scotland and Norway, and the south coasts of Greenland and Iceland [in Figs. 4a, Ea and Ef]). Moreover, local maxima in connection with the Rocky and Cantabrian mountains, the French and Dinaric alps, as well as Caucasus and the mountains of Japan point to the role of the water bodies to the west of these mountains [(Figs. 4a, Ea and Ef)]. As the westerly wind crosses these waters, the air gains moisture that later result in orographic precipitation on the windward side of the mountains as the air is forced upwards.

Frontal precipitation is represented reasonably well in NorESM and CCSM ([Figs. Ea and Ef compared to Fig. 4a, and Figs. 4a, Ea and Ef compared to Figs. 2a, Ca and Cf]). However, in the North Atlantic Ocean, both models give the precipitation field an orientation that is too zonal in the western half and too meridional in the eastern half. As a consequence, considerably more precipitation falls in the northeastern corner of the North Atlantic Ocean [in NorESM and CCSM compared to ERA-I (Figs. 4b and 4c)].

The orographic precipitation maxima at [storm track landfall] in the two models are shifted [inland] compared to ERA-I ([Figs. 4b and 4c]). This is likely a result of the resolution difference, in which elevation gradients are smoothed (i.e., weakened) over larger grid boxes. With a prevailing westerly wind in the domain, the air “feels” the mountains later (i.e., farther east) in NorESM and CCSM than in ERA-I. Moreover, the coarse resolution of NorESM restricts the ability to represent orographic precipitation, so the orographic maxima in NorESM are too weak (Fig. 4b).

New references:

Kunkel, K., Easterling, D., Kristovich, D., Gleason, B., Stoecker, L., and Smith, R.: Meteorological causes of the secular variations in observed extreme precipitation events for the conterminous United States, J. Hydrometeorology, 13, 1131–1141, doi:10.1175/JHM-D-11-0108.1, 2012.âĂĺ

Magnusdottir, G., Deser, C., and Saravanan, R.: The effects of North Atlantic SST and sea ice anomalies on the winter circulation in CCM3. Part I: Main features and storm track characteristics of the response, J. Climate, 17, 857–876, doi:10.1175/1520-0442(2004)017<0857:TEONAS>2.0.CO;2, 2004.âĂĺ

— 4: Wind changes —

Change of 1st paragraph in 3.1.3 Mean intensity (changes in [brackets]):

The average strength of cyclones per unit area is presented in [Figs. 3a, Da and Df. This is measured as mean intensity, indirectly linked to spatial changes in wind fields through the horizontal component of relative vorticity.] Since regions of numerous cyclones are likely also to include more intense cyclones than other regions, the mean intensity pattern generally follows the track density pattern in [Figs. 2a, Ca and Cf. Additionally,] cyclones are stronger over ocean than land. [Dependent clause deleted.]

Change of 5th paragraph in 3.2.2 Track density (changes in [brackets]):

The variability in the North Pacific storm track severely determines the day-to-day weather conditions [downstream] in the coastal regions of western Canada and southern Alaska. The same can be said of the North Sea region from the North Atlantic storm track, [both regions] represented by wet and [stormy] climates [in Figs. 2a, 3a and 4a. This feature explains the choice of regions shown in Fig. 6a. Some earlier studies have indicated poleward shifts of the two main storm tracks in a warmer climate (e.g., Bengtsson et al., 2006, 2009, Fischer-Bruns et al., 2005). If this also holds for NorESM and CCSM, we would expect to see track density reductions in WNA and NWE with corresponding enhancements in BWA and NEE. However, Table 3 shows no

clear indications of these shifts.]

Change of 5th paragraph in 4 Conclusions (changes in [brackets]):

[Storm frequency, intensity] and precipitation changes are likely to have costly impacts on human society, especially on top of sea level rise. This adds to the importance of reducing the uncertainties in future changes of Arctic cyclone activity and related variables that will impact northern coasts, communities and offshore activities.

New references:

Fischer-Bruns, I., von Storch, H., González-Rouco, J., and Zorita, E.: Modelling the variability of midlatitude storm activity on decadal to century time scales, Clim. Dynam., 25, 461–476, doi:10.1007/s00382-005-0036-1, 2005.

— 5: CMIP5 – ERA-I —

Please see — 3: Error discussion — above.

— 6: References storms impact on sea ice —

Change of 2nd paragraph in 1 Introduction (changes in [brackets]):

Much of the effort to diagnose and project Arctic change has focused on temperature, sea ice and precipitation. However, climate-driven changes in storms are arguably more important considerations for Arctic residents, as well as for the heat and moisture budgets of the atmosphere. The impacts of storms are magnified by the loss of sea ice, which increases wave activity, coastal flooding and erosion and also increases the risks of vessel icing in waters newly accessible for marine transport and for other offshore activities [(AMAP, 2005)].

New references:

AMAP: Arctic Climate Impact Assessment (ACIA), Tech. rep., Arctic Monitoring and Assessment Programme (AMAP), New York, USA, 2005.

— 7: Reference Karl et al. (2009) —

Change of 3rd paragraph and added new 4th paragraph in 1 Introduction (changes in [brackets]):

Analyses of observational data have produced mixed results on trends of high-latitude storminess. In earlier studies, Zhang et al. (2004) found an increase of Arctic cyclone activity, while McCabe et al. (2001) reported northward shifts of storm tracks over the Northern Hemisphere (NH) over the last several decades of the 20th century. Wang et al. (2006) detected a northward shift of cyclone activity, primarily during winter, over Canada during 1953–2002, and this meridional shift was confirmed more generally in a more recent study by the same group (Wang et al., 2013). The recent U.S. National Climate Assessment (Melillo et al., 2014) points to a poleward shift of storm tracks over the United States during recent decades. However, Mesquita et al. (2010) found that temporal trends of cyclones in the North Pacific Ocean have generally been weak over the 60-year period ending 2008. The U.S. Global Change Research Program (Karl et al., 2009) points to an increase of storminess on the northern Alaskan coast and to associated risks of flooding and coastal erosion [along with expected sea level rise]. Since any increases of coastal flooding and erosion are also related to retreating sea ice, [storms in coastal areas of the Arctic can pose increasing risks regardless of whether storm activity is changing].

[Previous work addressing cyclone-sea-ice linkages has shown increasing cyclone strength occurring with decreasing September sea ice edge, though no relationship with cyclone counts was found (Simmonds and Keay, 2009). Increasing amounts of open water in the Arctic enhance exchanges of heat, moisture, and momentum between the surface and atmosphere as a cyclone passes. Depending on the track of a cyclone, these additional fluxes can impact cyclone development. Two studies, one an evaluation of midlatitude marine cyclones (Kuo et al., 1991) and the other a case study of summer Arctic cyclones (Lynch et al., 2003), found surface energy flux input to be most important in the initial formation stages of the cyclone. Inputs in the later

stages of the cyclone life cycle showed little impact. Furthermore, two case studies of Arctic cyclones found that increased surface energy fluxes in the later stages of the cyclone were not enough to overcome the large-scale dynamics (Long and Perrie, 2012; Simmonds and Rudeva, 2012). However, the former study indicated increased maximum wind speeds as the cyclone studied moved over open water, primarily through enhanced momentum exchange between the surface and atmosphere compared to what would occur over sea ice. These results indicate that the cyclone track is rather important as to whether or not changing surface conditions will significantly impact cyclone development.]

New references:

Kuo, Y.-H., Shapiro, M., and Donall, E.: The interaction between baroclinic and diabatic processes in a numerical simulation of a rapidly intensifying extratropical marine cyclone, Mon. Weather Rev., 119, 368–384, doi:10.1175/1520-0493(1991)119<0368:TIBBAD>2.0.CO;2, 1991.

Lynch, A., Cassano, E., Cassano, J., and Lestak, L.: Case studies of high wind events in Barrow, Alaska: Climatological context and development processes, Mon. Weather Rev., 131, 719–732, doi:10.1175/1520-0493(2003)131<0719:CSOHWE>2.0.CO;2, 2003.

Simmonds, I. and Keay, K.: Extraordinary September Arctic sea ice reductions and their relationships with storm behavior over 1979–2008, Geophys. Res. Lett., 36, L19 715, doi:10.1029/2009GL039810, 2009.

Simmonds, I. and Rudeva, I.: The great Arctic cyclone of August 2012, Geophys. Res. Lett., 39, L23 709, doi:10.1029/2012GL054259, 2012.

Long, Z. and Perrie, W.: Air-sea interactions during an Arctic storm, J. Geophys. Res.-Atmos., 117, D15 103, doi:10.1029/2011JD016985, 2012.

— 8: Reference CMIP5 —

Change of 5th paragraph in 1 Introduction (changes in [brackets]):

Global climate models are arguably the best tools for identifying externally forced signals [(greenhouse gases and aerosols)] in storm activity. In this study, we seek to validate the storm track components of two state-of-the-art global climate models over midlatitudes and high-latitudes of the NH. This is done through a comparison to a reanalysis data set. The models are the Norwegian Earth System Model version 1 with intermediate resolution (NorESM1-M) and the Community Climate System Model version 4 (CCSM4). The simulations examined here were performed as part of the Coupled Model Intercomparison Project phase 5 (CMIP5[; Taylor et al., 2012]). After assessing the models' ability to capture the primary cyclone characteristics over a recent historical period, we compare the future changes of [high- and midlatitude] storms through the late 21st century. The primary metrics of storm activity will be frequency (track density) and intensity. [This evaluation is both a comparison between the time periods for each model and a model intercomparison on diverging changes towards the late 21st century.] The primary metrics of storm activity [here are] frequency (track density) and intensity [(mean intensity)].

New references:

Taylor, K., Stouffer, R., and Meehl, G.: An overview of CMIP5 and the experiment design, B. Am. Meteorol. Soc., 93, 485–498, doi:10.1175/BAMS-D-11-00094.1, 2012.

— 9: Resolution ERA-I —

Please see — 3: Error discussion — above.

Change of 7th-8th paragraph in 2 Data sets and methods (changes in [brackets]):

The analysis involves three time periods of 27 years each and two Representative Concentration Pathways (RCPs). For the historical time period, 1979–2005, NorESM and CCSM are compared to the European Re-Analysis Interim (ERA-Interim; here abbreviated ERA-I) data set (Dee et al., 2011). ERA-I is a high-resolution reanalysis

set in space and time[, and] is well suited for the northern regions (Jakobson et al., 2012; Chung et al., 2013), especially for storm tracking (Hodges et al., 2011; Zappa et al., 2013a).

[For the historical time period, the three data sets are interpolated to a 1° x 1° regular latitude-longitude grid for comparison. NorESM and CCSM historical means are also compared to future projections, albeit then on their respective native grids as these comparisons are rather between time periods than models.] The future time periods are 2037–2063 (mid-century) and 2074–2100 (end of the century). For these two periods, both RCP4.5 and RCP8.5 are analysed (van Vuuren et al., 2011). These represent pathways with stabilization without overshooting to 4.5 W m−2 by 2100, and continuous increase to 8.5 W m−2 by 2100, respectively.

— 10: SIE observations —

Change of 9th paragraph in 2 Data sets and methods (changes in [brackets]):

While the storm track analysis is based on 6-hourly zonal (u) and meridional (v) wind data, sea ice concentration (SIC), sea level pressure (SLP) and total precipitation (hereafter referred to simply as precipitation) examined here are monthly averages. All parameters are analysed over the extended autumn season September through December (SOND), which is the season of greatest ice retreat as shown in Table 1. The seasonal cycle of climatological monthly sea ice extent (SIE) for the [previous decade is captured by the two models, although both models show weaker seasonal cycles of ice retreat compared to the observational data from the National Snow and Ice Data Center (NSIDC; Fetterer et al., 2002, updated daily) (Table 1). Nevertheless, Langehaug et al. (2013) found the relative trends in NorESM to be close to those observed. In the coming decades,] CCSM simulates slightly more rapid ice retreat [than] NorESM, although both models show the Arctic Ocean becoming [seasonally] ice-free (SIE < 1 million km2) during the second half of the 21st century [(Table 1)]. The projected reduction of ice extent is greatest in the autumn and early winter, especially in terms of the

percentage reduction from the historical values. Even the areal reductions are largest during this portion of the year. Moreover, the observed ice loss during recent decades (1979–present) is also greatest during the autumn (Stroeve et al., 2012; Rogers et al., 2013). In view of this seasonality, we focus our analysis on the SOND season.

Update of Table 1 (caption changes in [brackets]):

<Table_1.pdf>

Table 1. Decadal mean Arctic sea ice extent monthly averages for 2000's, 2050's and 2090's and changes for the two latter decades compared to the former, following the RCP8.5 scenario. [2000's: First number within row from NSIDC; second number within row from NorESM; third number within row from CCSM. Other decades:] First number within each row from NorESM; second number within each row from CCSM. Unit [is] 10ˆ6 km2.

New references:

Fetterer, F., Knowles, K., Meier, W., and Savoie, M.: Sea Ice Index, Version 1, doi:10.7265/N5QJ7F7W, digital media, 2002, updated daily.

— 11: ζ vs. SLP — Please see — 3: Error discussion — above.

Change of 10th paragraph in 2 Data sets and methods (changes in [brackets]):

The storm track analysis is based on the TRACK algorithm described by Hodges (1994, 1995, 1999). It uses 6-hourly 850-hPa relative vorticity (ζ) to identify and track cyclones, here calculated from the u and v fields. Rather than SLP, ζ is used for tracking due to the [focus on storminess. ζ contains more information on the wind field and the high-frequency range of the synoptic scale, whereas SLP is linked to the mass field and represents the low-frequency scale better (Hodges et al., 2003). This results in generally more cyclones identified using vorticity tracking (Hodges et al., 2011).] Overall, Neu et al. (2013) found the number of storms identified by methods based on vorticity to be in the middle range of those obtained using different tracking algorithms.

— 12: Clarification reference Tilinina et al. (2014) —

Change of 5th paragraph in 3.1.2 Track density (changes in [brackets]):

Moreover, most of the discrepancy relative to ERA-I stems from the high-latitudes south of the Arctic Ocean, with 14 % more cyclones in CCSM over the band 55–65°N [(Fig. 2c)]. This [points] to a closer similarity of CCSM to the Arctic System Reanalysis (ASR) over ERA-I, as found by Tilinina et al. (2014). They detected 28–40 % more cyclones over high-latitude continental areas in summer and winter in the ASR compared to ERA-I and other global modern era reanalyses, ascribing the anomaly mostly to moderately deep and shallow cyclones [(cyclones with central pressure higher than 980 hPa)].

— 13: Clarification mean intensity and temperature —

Change of 1st paragraph in 3.1.3 Mean intensity (changes in [brackets]):

The average strength of cyclones per unit area is presented in [Figs. 3a, Da and Df. This is measured as mean intensity, indirectly linked to spatial changes in wind fields through the horizontal component of relative vorticity.] Since regions of numerous cyclones are likely also to include more intense cyclones than other regions, the mean intensity pattern generally follows the track density pattern in [Figs. 2a, Ca and Cf. Additionally, cyclones] are stronger over ocean than land. [Dependent clause deleted.]

— 14: Frontal precipitation in Fig. 4 —

Change of 1st-2nd paragraph and added new 7th paragraph in 3.1.4 Precipitation (changes in [brackets]):

[In terms of broad-scale pattern, precipitation is positively correlated with storminess, although one cannot say that precipitation is a real measure of storminess. Hawcroft et al. (2012) and Catto et al. (2012) showed the proportion of precipitation associated with extratropical cyclones and fronts, respectively. Only through this type of linkage can a causal relationship be established. In this study, because precipitation per se is not our

main focus, we merely point to consistencies between our results and general characteristics of precipitation vis-à-vis its drivers. For example,] cyclone-dense regions are [generally] characterized by high frontal precipitation, with precipitation reaching [especially] high levels [where] cyclones track into mountainous land [so that precipitation is orographically enhanced].

[Figures 4a, Ea and Ef] show the average pattern of precipitation for NH midlatitudes and high-latitudes over the historical time period. [While climate models generally distinguish convective and non-convective precipitation, their archives do not distinguish frontal and orographic precipitation – two of the primary types of non-convective precipitation. Nevertheless, one can infer that heavy precipitation events in non-mountainous areas have a general association with frontal activity (Kunkel et al. 2012), while precipitation maxima in mountainous areas have a substantial orographic component. Subject to these assumptions, some inferences can be made about the key features that stand out in Fig. 4.] [Sentence moved.] [The discussed connection between total precipitation and cyclone frequency and strength is based on an assumption that frontal precipitation is well captured in models. However, Stephens et al. (2010) found that climate models generally overestimate the frequency and underestimate the intensity of precipitation. These compensating errors were discussed in more detail by Catto et al. (2013), who found them largely to be driven by the non-frontal precipitation regimes. These findings are consistent with the biases in NorESM and CCSM.]

Change of 2nd paragraph in 3.2.4 Precipitation (changes in [brackets]):

[The reduced precipitation in the eastern North Atlantic Ocean in September coincides with reduced cyclone frequency in CCSM and intensity in both NorESM and CCSM (Figs. 8a and 8b compared to Figs. 6b, 7a and 7b). The correspondence between precipitation and cyclone intensity is consistent with the findings of Zappa et al. (2013b). However, while the changes in storm tracks and precipitation are coherent, this consistency does not prove a causal relationship. The expected drying of the eastern North Atlantic Ocean stems from the poleward migration of the Hadley Cell's downward limb

(Kang and Lu, 2012), which is projected to increase dryness in the African-Eurasian region (including the Mediterranean), southwestern North America and northeastern Brazil (Lau and Kim, 2015). The eastern North Atlantic] is projected to warm less than the rest of the NH, with relatively lower humidity [reducing the] potential for increased atmospheric moisture (Stocker et al., 2013). [In December, the changes of precipitation in the eastern North Atlantic are mostly positive and are not strongly related to storm track changes (Figs. 8c and 8d).]

New references:

Catto, J., Jakob, C., Berry, G., and Nicholls, N.: Relating global precipitation to atmospheric fronts, Geophys. Res. Lett., 39, L10 805, doi:10.1029/2012GL051736, 2012.

Catto, J., Jakob, C., and Nicholls, N.: A global evaluation of fronts and precipitation in the ACCESS model, Aust. Meteorol. Ocean. Soc. J, 63, 191–203, 2013.

Hawcroft, M., Shaffrey, L., Hodges, K., and Dacre, H.: How much Northern Hemisphere precipitation is associated with extratropical cyclones?, Geophys. Res. Lett., 39, L24 809, doi:10.1029/2012GL053866, 2012.

Kang, S. and Lu, J.: Expansion of the Hadley cell under global warming: Winter versus summer, J. Climate, 25, 8387–8393, doi:10.1175/JCLI-D-12-00323.1, 2012.

Kunkel, K., Easterling, D., Kristovich, D., Gleason, B., Stoecker, L., and Smith, R.: Meteorological causes of the secular variations in observed extreme precipitation events for the conterminous United States, J. Hydrometeorology, 13, 1131–1141, doi:10.1175/JHM-D-11-0108.1, 2012.

Lau, W. and Kim, K.-M.: Robust Hadley Circulation changes and increasing global dryness due to CO2 warming from CMIP5 model projections, P. Natl. Acad. Sci. USA, 112, 3630–3635, doi:10.1073/pnas.1418682112, 2015.

Stephens, G., L'Ecuyer, T., Forbes, R., Gettlemen, A., Golaz, J.-C., Bodas-Salcedo, A., Suzuki, K., Gabriel, P., and Haynes, J.: Dreary state of precipitation in global models,

J. Geophys. Res.-Atmos., 115, D24 211, doi:10.1029/2010JD014532, 2010.

Zappa, G., Shaffrey, L., Hodges, K., Sansom, P., and Stephenson, D.: A multimodel assessment of future projections of North Atlantic and European extratropical cyclones in the CMIP5 climate models*, J. Climate, 26, 5846–5862, doi:10.1175/JCLI-D-12-00573.1, 2013b.

— 15: Precipitation bias in GCMs —

Added new 7th paragraph in 3.1.4 Precipitation (new text in [brackets]):

[The discussed connection between total precipitation and cyclone frequency and strength is based on an assumption that frontal precipitation is well captured in models. However, Stephens et al. (2010) found that climate models generally overestimate the frequency and underestimate the intensity of precipitation. These compensating errors were discussed in more detail by Catto et al. (2013), who found them largely to be driven by the non-frontal precipitation regimes. These findings are consistent with the biases in NorESM and CCSM.]

New references:

Catto, J., Jakob, C., and Nicholls, N.: A global evaluation of fronts and precipitation in the ACCESS model, Aust. Meteorol. Ocean. Soc. J, 63, 191–203, 2013.

Stephens, G., L'Ecuyer, T., Forbes, R., Gettlemen, A., Golaz, J.-C., Bodas-Salcedo, A., Suzuki, K., Gabriel, P., and Haynes, J.: Dreary state of precipitation in global models, J. Geophys. Res.-Atmos., 115, D24 211, doi:10.1029/2010JD014532, 2010.

— 16: Precipitation, track density and mean intensity changes in eastern North Atlantic Ocean and the Mediterranean Sea —

Change of 2nd-4th paragraph in 3.2.4 Precipitation (changes in [brackets]):

[The reduced precipitation in the eastern North Atlantic Ocean in September coincides with reduced cyclone frequency in CCSM and intensity in both NorESM and CCSM

(Figs. 8a and 8b compared to Figs. 6b, 7a and 7b). The correspondence between precipitation and cyclone intensity is consistent with the findings of Zappa et al. (2013b). However, while the changes in storm tracks and precipitation are coherent, this consistency does not prove a causal relationship. The expected drying of the eastern North Atlantic Ocean stems from the poleward migration of the Hadley Cell's downward limb (Kang and Lu, 2012), which is projected to increase dryness in the African-Eurasian region (including the Mediterranean), southwestern North America and northeastern Brazil (Lau and Kim, 2015). The eastern North Atlantic] is projected to warm less than the rest of the NH, with relatively lower humidity [reducing the] potential for increased atmospheric moisture (Stocker et al., 2013). [In December, the changes of precipitation in the eastern North Atlantic are mostly positive and are not strongly related to storm track changes (Figs. 8c and 8d).]

The largest increases in precipitation are found along the shifted main storm tracks and in regions of enhanced cyclone frequency and strength (Figs. 6 and 7), in accordance with the near doubling along the cyclone tracks relative to the global mean increase found by Bengtsson et al. (2009). At the landfall of the shifted storm tracks, western Alaska and northern Scandinavia are projected to see much stormier and wetter autumns by the end of the century.

[Compared to September, the two models predict enhanced precipitation over more of the domain in December (Figs. 8c and 8d).] Part of the reason is [that] the [indication of a poleward shift of the storm tracks] is more significant for September than December (Sects. 3.2.2 and 3.2.3). [As in Zappa et al. (2014a), the expected drier conditions in the Mediterranean region coincide with a reduction in cyclone frequency (Fig. 6 compared to Fig. 8).] This is indicative of the wet-get-wetter, dry-get-drier pattern reported elsewhere (e.g., Held and Soden, 2006; Stocker et al., 2013).

New references:

Kang, S. and Lu, J.: Expansion of the Hadley cell under global warming: Winter versus

summer, J. Climate, 25, 8387–8393, doi:10.1175/JCLI-D-12-00323.1, 2012.

Lau, W. and Kim, K.-M.: Robust Hadley Circulation changes and increasing global dryness due to CO2 warming from CMIP5 model projections, P. Natl. Acad. Sci. USA, 112, 3630–3635, doi:10.1073/pnas.1418682112, 2015.

Zappa, G., Shaffrey, L., Hodges, K., Sansom, P., and Stephenson, D.: A multimodel assessment of future projections of North Atlantic and European extratropical cyclones in the CMIP5 climate models*, J. Climate, 26, 5846–5862, doi:10.1175/JCLI-D-12-00573.1, 2013b.

Zappa, G., Hawcroft, M., Shaffrey, L., Black, E., and Brayshaw, D.: Extratropical cyclones and the projected decline of winter Mediterranean precipitation in the CMIP5 models, Clim. Dynam., 45, 1–12, doi:10.1007/s00382-014-2426-8, 2014.

— 17: Sea ice retreat seasonality —

Please note that the 1st bullet point in 4 Conclusion refers to Table 1.

Added new 6th paragraph in 1 Introduction (new text in [brackets]):

[The impacts of a warming climate on high-latitude storms are difficult to anticipate. Both models undergo Arctic-amplified warming at low levels associated with significant loss of sea ice cover in the 21st century simulations examined here. On the one hand, the increased surface fluxes of heat and moisture might be expected to fuel more and stronger storms. On the other hand, the polar amplification decreases the low-level meridional temperature gradients, reducing the potential for storm activity. Nevertheless, because upper-level temperatures show greater increases in the tropics than in the Polar Regions, upper-level meridional temperature gradients actually increase (Harvey et al., 2015). Hence, the net effect on baroclinicity cannot be simply related to baroclinic disturbances such as extratropical cyclones (Ulbrich et al., 2009). Moreover, the Arctic amplification affects the variability of the jet stream, which is directly linked to the vertically integrated meridional temperature gradient via the thermal wind

equation. Barnes and Screen (2015) provide a diagnostic assessment of these connections. Here, the model set-up implies that impacts of Arctic warming, sea ice loss and changes in surface fluxes and temperature gradients are implicit in our results.]

Change of 1st bullet point in 4 Conclusions (changes in [brackets]):

The ongoing and projected retreat of sea ice is greatest in autumn, [creating the potential for increased fluxes of sensible and latent heat to from the surface to the atmosphere during these months].

New references:

Barnes, E. and Screen, J.: The impact of Arctic warming on the midlatitude jet-stream: Can it? Has it? Will it?, WIREs Clim. Change, 6, 277–286, doi:10.1002/wcc.337, 2015.

Harvey, B., Shaffrey, L., and Woollings, T.: Deconstructing the climate change response of the Northern Hemisphere wintertime storm tracks, Clim. Dynam., 45, 2847–2860, doi:10.1007/s00382-015-2510-8, 2015.

Ulbrich, U., Leckebusch, G., and Pinto, J.: Extra-tropical cyclones in the present and future climate: a review, Theor. Appl. Climatol., 96, 117–131, doi:10.1007/s00704-008-0083-8, 2009.

— 18: SLP and cyclone metrics biases and model resolution —

Please note that the 2nd bullet point in 4 Conclusion states that the track density and mean intensity biases are expected to decrease with increasing model resolution.

The statement referring to DeWeaver and Bitz (2006) in 3.1.1 Sea level pressure (that SLP bias was more pronounced in T85 compared to T42) refers to SLP.

— 19: Linear scaling with RCP forcing scenario and time —

Please see — 1: RCP4.5 and 2037-2063 inclusions — above.

— 20: Diminishing sea ice cover and storm track implications —

Please see the changes to the text reproduced below.

We agree with the reviewer that a more explicit analysis between changes in sea ice cover, sea level pressure and storm tracks is of high scientific interest. However, as the main focus in this manuscript is on representation of storminess in NorESM in historical and future climate, we consider such an analysis outside the scope of this study.

Added new 6th paragraph in 1 Introduction (new text in [brackets]):

[The impacts of a warming climate on high-latitude storms are difficult to anticipate. Both models undergo Arctic-amplified warming at low levels associated with significant loss of sea ice cover in the 21st century simulations examined here. On the one hand, the increased surface fluxes of heat and moisture might be expected to fuel more and stronger storms. On the other hand, the polar amplification decreases the low-level meridional temperature gradients, reducing the potential for storm activity. Nevertheless, because upper-level temperatures show greater increases in the tropics than in the Polar Regions, upper-level meridional temperature gradients actually increase (Harvey et al., 2015). Hence, the net effect on baroclinicity cannot be simply related to baroclinic disturbances such as extratropical cyclones (Ulbrich et al., 2009). Moreover, the Arctic amplification affects the variability of the jet stream, which is directly linked to the vertically integrated meridional temperature gradient via the thermal wind equation. Barnes and Screen (2015) provide a diagnostic assessment of these connections. Here, the model set-up implies that impacts of Arctic warming, sea ice loss and changes in surface fluxes and temperature gradients are implicit in our results.]

Added new 6th-7th paragraphs in 3.2.2 Track density (new text in [brackets]):

[No significant changes are found in NEE (Table 3 and Figs. 6a and 6c). Rather, both NorESM and CCSM show weak reductions in NEE track density (-11.6 to -0.8 %; Table 3) associated with enhancements in the Greenland Sea in September (Figs. 6a and 6b). Fig. A reveals that the latter increase coincides with a sea ice retreat in the Greenland Sea over the century. These results follow those of Deser et al. (2000),

Magnusdottir et al. (2004) and Knudsen et al. (2015), who found storm activity to be very sensitive to the sea ice variations east of Greenland. Moreover, Chen et al. (2015) showed a corresponding sensitivity in synoptic activity here associated with variations in the surface mass balance of the Greenland Ice Sheet.]

[Corresponding to the observed trend found by Sepp and Jaagus (2011), the raised number of cyclones tracking through the Greenland Sea coincides with an increase also in the Labrador Sea and Baffin Bay. While the additional cyclones in these regions are short-lived in CCSM (not shown), they continue polewards (not shown) and add to the projected Arctic Ocean cyclonic activity increase from the Pacific sector in NorESM (Fig. 6a). Nevertheless, this Arctic enhancement is found in September for NorESM alone, and the high-latitude circumglobal changes over the whole season in both models are negligible (-0.8 to +0.3 %; Table 2). This contrasts Harvey et al. (2015), who found a significant decrease in high-latitude storm activity with retreating sea ice edge, thus highlighting the complex interconnections determining synoptic changes in a warmer climate system.]

Change of 4th bullet point in 4 Conclusions (changes in [brackets]):

A significant projected decrease of the SLP over the Arctic Ocean during the 21st century [appears to be] partly a consequence of the diminishing sea ice cover on the same time scales. [These changes are consistent with increased heating of the lower troposphere over areas of sea ice loss, resulting in increased thicknesses in the lower troposphere, and increased geopotential heights and mass divergence aloft. Accordingly, sea level pressures] are projected to [decrease over the Arctic Ocean and] increase farther south, significantly over the North Atlantic Ocean, [coinciding] with [reduced mid-latitude] storm [track activity].

New references:

Barnes, E. and Screen, J.: The impact of Arctic warming on the midlatitude jet-stream: Can it? Has it? Will it?, WIREs Clim. Change, 6, 277–286, doi:10.1002/wcc.337, 2015.

Chen, L., Fettweis, X., Knudsen, E., and Johannessen, O.: Impact of cyclonic and anticyclonic activity on Greenland ice sheet surface mass balance variation during 1980–2013, Int. J. Climatol., doi:10.1002/joc.4565, 2015.

Deser, C., Walsh, J., and Timlin, M.: Arctic sea ice variability in the context of recent atmospheric circulation trends, J. Climate, 13, 617–633, doi:10.1175/1520-0442(2000)013<0617:ASIVIT>2.0.CO;2, 2000.

Harvey, B., Shaffrey, L., and Woollings, T.: Deconstructing the climate change response of the Northern Hemisphere wintertime storm tracks, Clim. Dynam., 45, 2847–2860, doi:10.1007/s00382-015-2510-8, 2015.

Knudsen, E., Orsolini, Y., Furevik, T., and Hodges, K.: Observed anomalous atmospheric patterns in summers of unusual Arctic sea ice melt, J. Geophys. Res.-Atmos., 120, 2595–2611, doi:10.1002/2014JD022608, 2015.

Magnusdottir, G., Deser, C., and Saravanan, R.: The effects of North Atlantic SST and sea ice anomalies on the winter circulation in CCM3. Part I: Main features and storm track characteristics of the response, J. Climate, 17, 857–876, doi:10.1175/1520-0442(2004)017<0857:TEONAS>2.0.CO;2, 2004.

Ulbrich, U., Leckebusch, G., and Pinto, J.: Extra-tropical cyclones in the present and future climate: a review, Theor. Appl. Climatol., 96, 117–131, doi:10.1007/s00704-008-0083-8, 2009.

Please also note the supplement to this comment:
http://www.geosci-model-dev-discuss.net/7/C3799/2016/gmdd-7-C3799-2016-supplement.pdf

---

Interactive comment on Geosci. Model Dev. Discuss., 7, 8975, 2014.

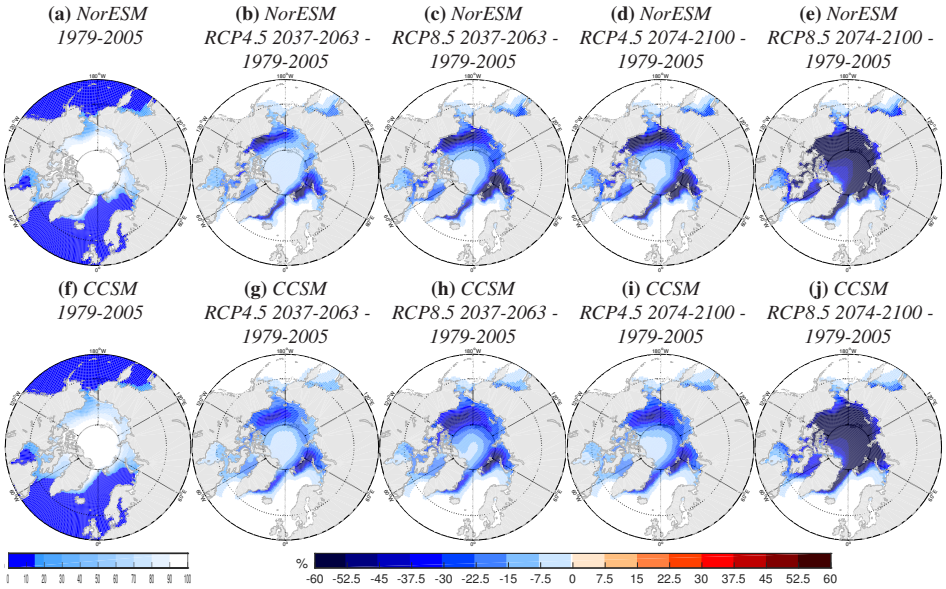

Fig. 1. New Figure A. Please see supplement or — 1: RCP4.5 and 2037-2063 inclusions — for caption.

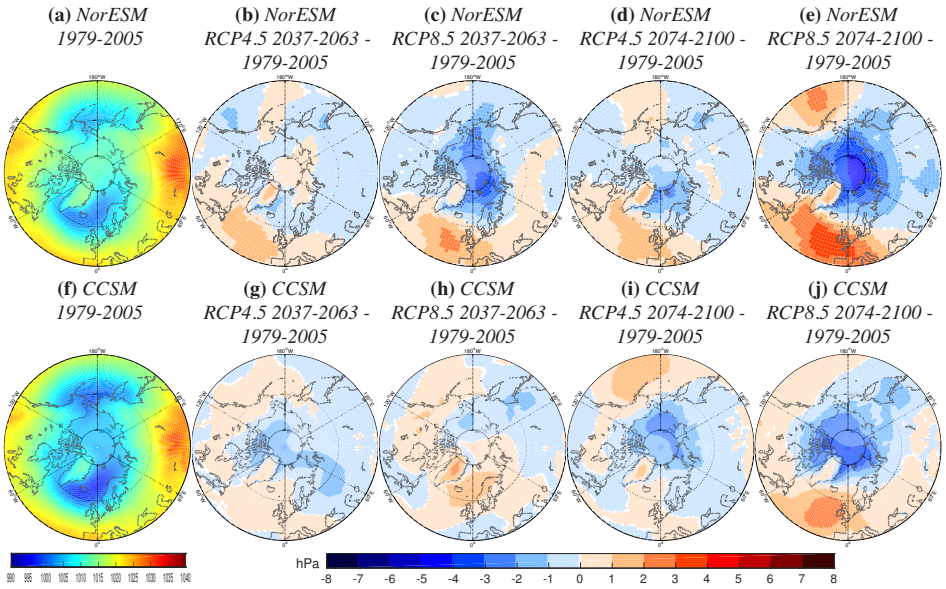

Fig. 2. New Figure B. Please see supplement or — 1: RCP4.5 and 2037-2063 inclusions — for caption.

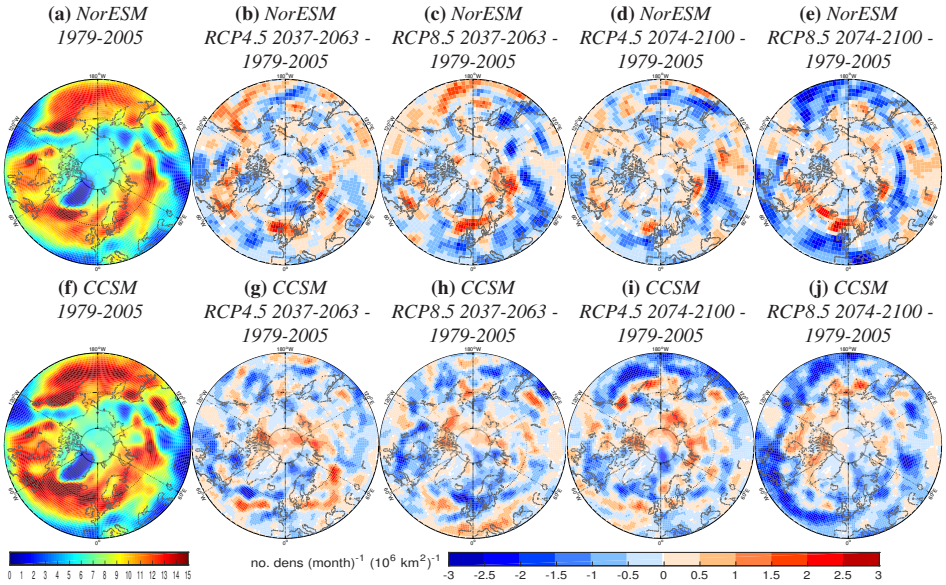

Fig. 3. New Figure C. Please see supplement or — 1: RCP4.5 and 2037-2063 inclusions — for caption.

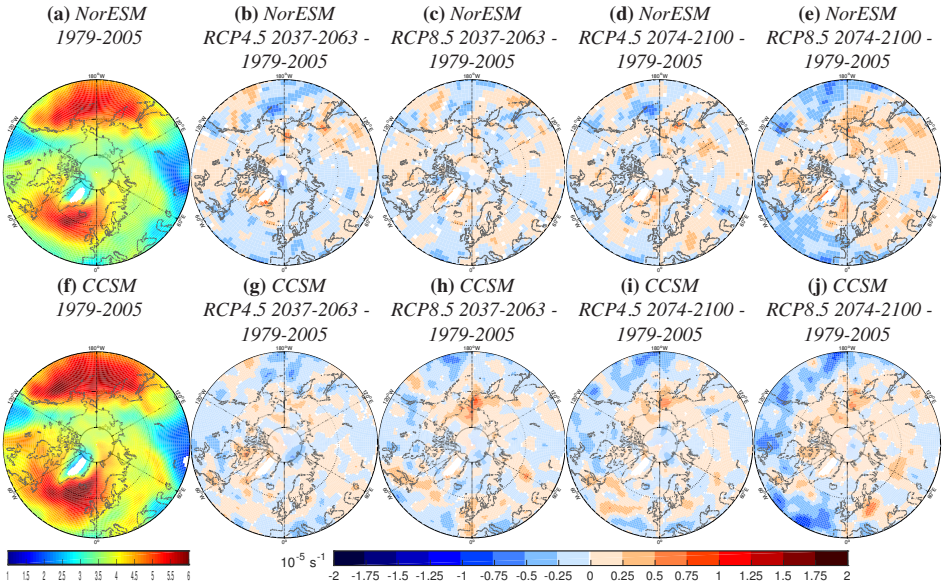

Fig. 4. New Figure D. Please see supplement or — 1: RCP4.5 and 2037-2063 inclusions — for caption.

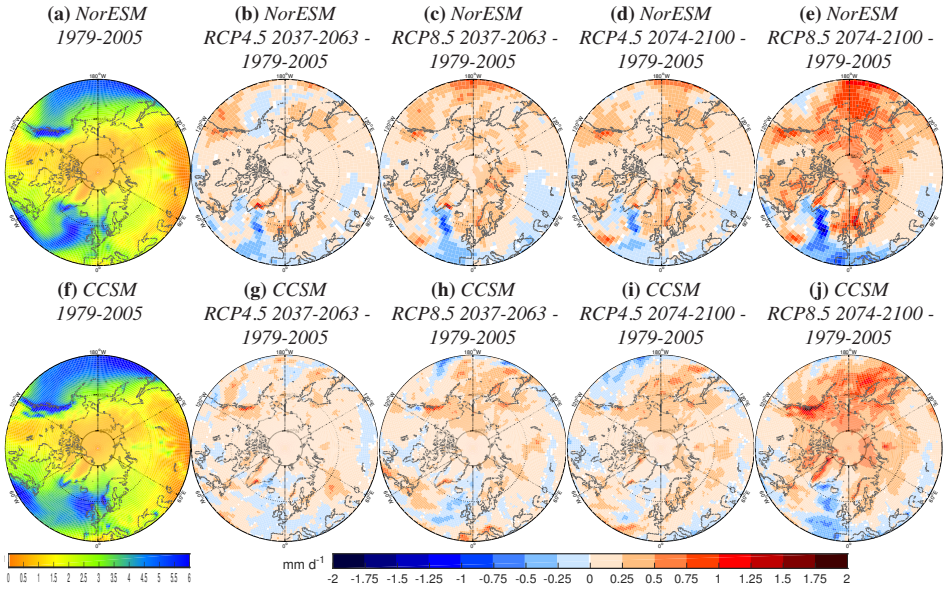

Fig. 5. New Figure E. Please see supplement or — 1: RCP4.5 and 2037-2063 inclusions — for caption.

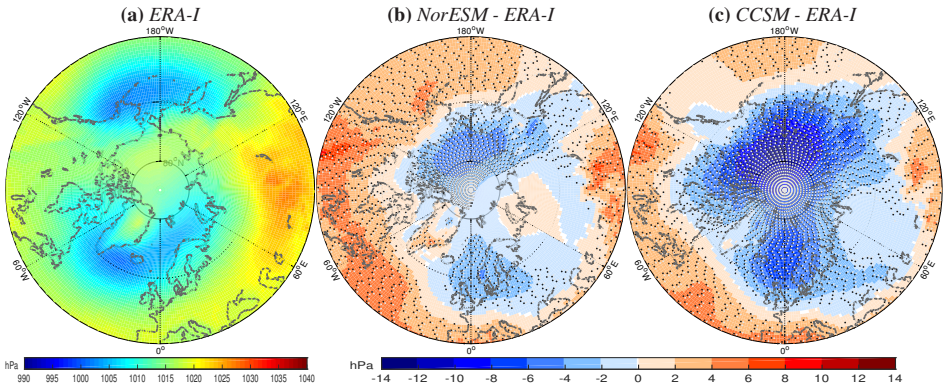

Fig. 6. Changed Figure 1. Please see supplement or — 3: Error discussion — for caption.

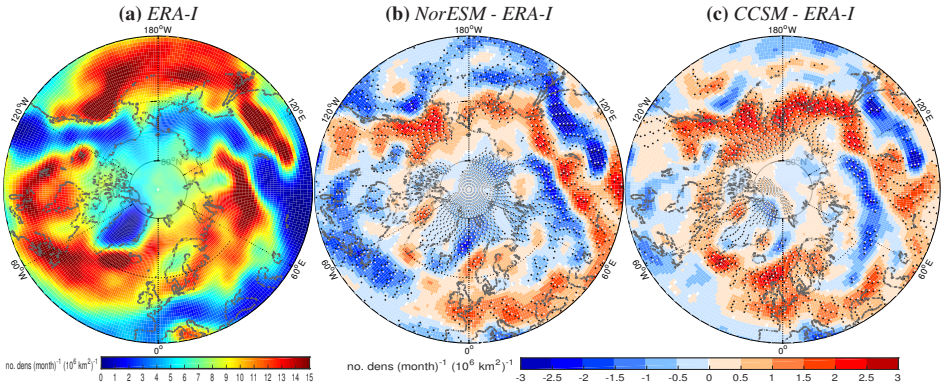

Fig. 7. Changed Figure 2. Please see supplement or — 3: Error discussion — for caption.

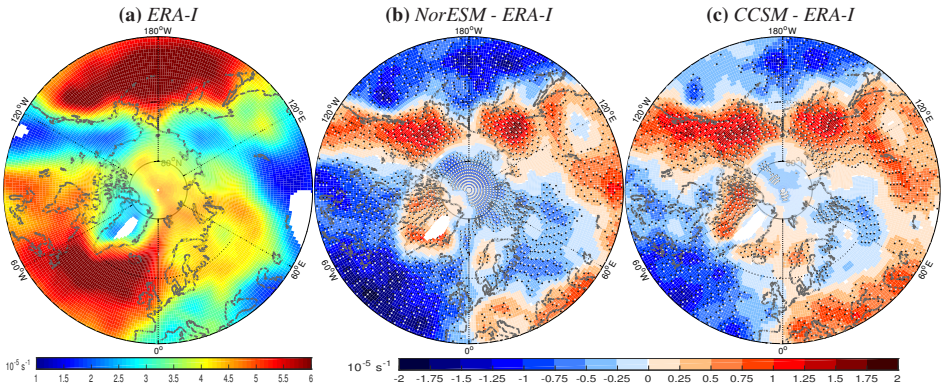

Fig. 8. Changed Figure 3. Please see supplement or — 3: Error discussion — for caption.

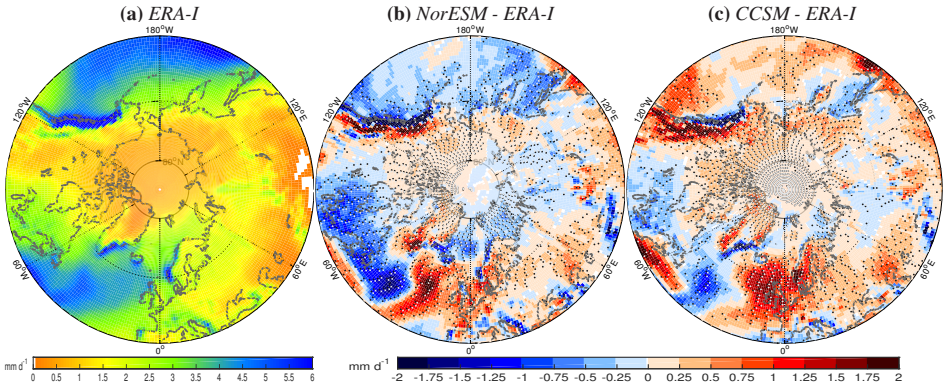

Fig. 9. Changed Figure 4. Please see supplement or — 3: Error discussion — for caption.

Table 1. Decadal mean Arctic sea ice extent monthly averages for 2000's, 2050's and 2090's and changes for the two latter decades compared to the former, following the RCP8.5 scenario. **2000's: First number within row from NSIDC; second number within row from NorESM; third number within row from CCSM. Other decades:** First number within each row from NorESM; second number within each row from CCSM. Unit **is** 10^6 km^2.

Decade	Jan	Feb	Mar	Apr	May	Jun	Jul	Aug	Sep	Oct	Nov	Dec
	14.1	14.9	15.1	14.3	13.1	11.5	9.1	6.5	5.7	8.3	10.4	12.6
2000's	13.1	14.0	14.7	14.2	13.3	11.7	10.2	9.0	7.8	9.2	10.6	12.1
	12.4	13.0	13.2	12.8	11.9	10.4	8.7	6.6	5.5	7.3	8.8	10.8
2050's	10.7	11.9	12.7	12.5	11.5	9.9	8.3	6.9	5.5	6.0	7.1	8.9
	10.0	10.8	11.2	10.8	10.3	9.1	5.3	0.8	0.8	1.1	4.4	7.8
2090's	8.8	10.1	11.1	11.0	9.7	7.6	4.8	2.3	0.3	1.4	3.7	6.2
	6.6	9.1	9.9	9.8	9.3	7.2	1.7	0	0	0	0.3	2.8
Δ2050's	-2.4	-2.1	-2.0	-1.7	-1.8	-1.8	-1.9	-2.1	-2.3	-3.2	-3.5	-3.2
	-2.4	-2.2	-2.0	-2.0	-1.6	-1.3	-3.4	-5.8	-4.7	-6.2	-4.4	-3.0
Δ2090's	-4.3	-3.9	-3.6	-3.2	-3.6	-4.1	-5.4	-6.7	-7.5	-7.8	-6.9	-5.9
	-5.8	-3.9	-3.3	-3.0	-2.6	-3.2	-7.0	-6.6	-5.5	-7.3	-8.5	-8.0

Fig. 10. Changed Table 1. Please see supplement or — 10: SIE observations — for caption.